P3H-22-090
SI-HEP-2022-21
TTP22-056
Nikhef 2022-010
August 9, 2022

New physics contributions to moments of inclusive $b \to c$ semileptonic decays

Matteo Fael[a], Muslem Rahimi[b], and K. Keri Vos[c,d]

[a] *Institut für Theoretische Teilchenphysik Karlsruhe Institute of Technology (KIT), 76128 Karlsruhe, Germany*

[b] *Center for Particle Physics Siegen (CPPS), Theoretische Physik 1, Universität Siegen, 57068 Siegen, Germany*

[c] *Gravitational Waves and Fundamental Physics (GWFP), Maastricht University, Duboisdomein 30, NL-6229 GT Maastricht, the Netherlands*

[d] *Nikhef, Science Park 105, NL-1098 XG Amsterdam, the Netherlands*

Abstract

Inclusive semileptonic $B \to X_c \ell \bar{\nu}_\ell$ decays, where $\ell = \mu, e$, are by now standard candles in the determination of the CKM element $|V_{cb}|$. These determinations rely on the heavy-quark expansion and use moments of decay spectra to extract the non-perturbative parameters directly from data under the standard model assumption.

At the same time, new physics could influence the moments of the inclusive decay. In this paper, we compute power-corrections and next-to-leading order corrections in the strong coupling constant using the full basis of dimension-six new physics operators for the inclusive $B \to X_c \ell \bar{\nu}$ decay. We provide predictions for lepton energy, hadronic and leptonic invariant mass moments, and perform a phenomenological study to show the possible impact of new physics. Our results could be used to perform a global fit including new physics contributions.

1 Introduction

Semileptonic $b \to c$ decays provide important tests of the Standard Model (SM) of particle physics as they are mediated by a tree-level weak transition. As such, both the inclusive $B \to X_c \ell \bar{\nu}_\ell$ and exclusive $B \to D^{(*)} \ell \bar{\nu}_\ell$ decays, where $\ell = \mu, e$, are clean probes of the CKM element $|V_{cb}|$. For the exclusive decays, this requires information on the $B \to D^{(*)}$ form factors, while the inclusive decay relies fully on the heavy quark expansion (HQE) and the extraction of non-perturbative parameters from data. Thanks to a combined theoretical and experimental effort, the inclusive determination of $|V_{cb}|$ has reached an impressive $1.2-1.5\%$ relative uncertainty [1, 2].

Despite this progress, the puzzling tension between the exclusive and inclusive determination of V_{cb} persists and has received quite some attention recently (see e.g. [3–9]). At the same time the possible New Physics (NP) origin of this discrepancy has been investigated (see [10–12]). The search for such NP has been boosted by the recent finding of the B anomalies, discrepancies between experimental data and theoretical SM predictions in both the neutral ($b \to s\ell\ell$) and charged ($b \to c\tau\bar{\nu}_\tau$) current decay of B mesons.

In this paper, we consider the effect of possible new physics interactions on moments of the inclusive $B \to X_c \ell \bar{\nu}_\ell$ decay, for light leptons. The effect of NP on the moments of the $b \to c$ spectrum have so far only been studied in [13, 14], where a subset of possible NP operators was included. NP contributions to the total inclusive rate were included in the analysis of Ref. [11], while new tensor interactions were discussed in [10].

Using the framework of the HQE, we consider the $B \to X_c \ell \bar{\nu}_\ell$ spectra including the full set of NP dimension-six operators appearing in the weak effective theory (WET) below the electroweak (EW) scale. We provide predictions for lepton energy (E_ℓ), hadronic (M_X^2) and leptonic (q^2) invariant mass moments. Moreover we study also NP effects in forward-backward asymmetries which were proposed in [15] and recently reconsidered in [16]. When considering the most general effective Hamiltonian for $b \to c\ell\bar{\nu}_\ell$ transition with dimension-six operators, we have three expansion parameters in the HQE: the inverse of the EW scale $G_F = 1/(\sqrt{2}v^2)$, $1/m_b$ and $\alpha_s(m_b)$. In order to properly catch the leading effects in the various moments, we compute the following kind of contributions:

- NP contributions at tree level in the free-quark approximation. These terms scale like $G_F^2 \times \alpha_s^0 \times (\frac{1}{m_b})^0$ in the prediction for the differential rate. Note that the interference between SM and NP operators vanishes for scalar and tensor currents when the leptons are considered massless.

- Power suppressed contributions up to order $1/m_b^3$ also for the NP operator contributions. These corrections scale like $G_F^2 \times \alpha_s^0 \times (\frac{1}{m_b})^{2,3}$. Since the prediction for q^2 and M_X^2 central moments receive large contributions from power corrections, it is important to consider also the power suppressed terms for the NP effects.

- Perturbative QCD NLO corrections to the NP effective interactions in the free quark approximation, which scale like $G_F^2 \times \alpha_s^1 \times (\frac{1}{m_b})^0$. For the second and third central

moments of M_X^2, the α_s corrections are effectively a leading-order contribution since the partonic invariant mass differs from m_c only starting at $\mathcal{O}(\alpha_s)$.

In the end, our results could be included in a fit to the experimental data to constrain possible NP contributions. We plan to implement this in the EOS software [17]. In the mean time, to show the impact of such an analysis, we illustrate the effect of different NP scenarios with some phenomenological studies. Finally, we present a toy fit to show the effect on the V_{cb} extraction, as the HQE parameters could mimic the effect of NP.

This work is organised as follows. In Section 2 we introduce the set of dimension-six operators which can contribute to the inclusive semileptonic B decay and discuss the derivation of the NLO corrections for the NP operators. In Sec. 3 we present the results for the NP contributions to moments, illustrate their effects using three benchmark scenarios and study their impact on the extraction of the HQE parameters in global fits via a toy fit. In Sec. 4 we discuss the effects of NP in the forward-backward asymmetries. We conclude in Sec. 5. In Appendix A, we give the contribution to the total rate, while in Appendix B we give our results for the different contributions to the moments.

2 Effective NP contributions to $b \to c\ell\bar{\nu}_\ell$

We consider NP effects in $b \to c\ell\bar{\nu}_\ell$ decays arising from

$$\mathcal{H}_{\text{eff}} = \frac{4G_F V_{cb}}{\sqrt{2}} \left[(1 + C_{V_L})\, O_{V_L} + \sum_{i=V_R,S_L,S_R,T} C_i\, O_i \right], \tag{1}$$

where the effective dimension-six operators are

$$O_{V_{L(R)}} = \left(\bar{c}\gamma_\mu P_{L(R)} b\right) \left(\bar{\ell}\gamma^\mu P_L \nu_\ell\right) , \tag{2}$$

$$O_{S_{L(R)}} = \left(\bar{c} P_{L(R)} b\right) \left(\bar{\ell} P_L \nu_\ell\right) \tag{3}$$

$$O_T = \left(\bar{c}\,\sigma_{\mu\nu} P_L b\right) \left(\bar{\ell}\,\sigma^{\mu\nu} P_L \nu_\ell\right) . \tag{4}$$

with $P_{L(R)} = 1/2\,(1 \mp \gamma_5)$ and $\sigma^{\mu\nu} = \frac{i}{2}[\gamma^\mu, \gamma^\nu]$. In the SM only O_{V_L} contributes. We have written out this contribution explicitly, such that all Wilson coefficients C_i are zero in the SM. We do not consider interactions with right handed neutrinos (see e.g. [18] for a discussion of these effects on exclusive $B \to D^{(*)}\ell\bar{\nu}_\ell$ decays).

Note that if one would consider NP effects in the SMEFT framework [19], there would be an additional expansion in powers of $1/\Lambda$, where Λ corresponds to the NP scale above the EW scale. The tree-level matching of SMEFT operators onto the effective Hamiltonian can be obtained from [20]. In the WET the expansion parameter is $1/v$, therefore from the SMEFT point of view the Wilson coefficients in Eq. (1) would be further suppressed by the small ratio $(v/\Lambda)^2$.

To study the effects of the NP operators on moments of the spectrum, we calculate the triple differential decay rate in terms of the lepton (neutrino) energy $E_{\ell(\nu)}$ and the dilepton

invariant mass $q^2 = (p_\ell + p_\nu)^2$. We write

$$\frac{\mathrm{d}\Gamma_{\mathrm{SM+NP}}}{\mathrm{d}E_\ell \mathrm{d}q^2 \mathrm{d}E_\nu} = \frac{G_F^2 |V_{cb}|^2}{16\pi^3} \tilde{W} \otimes \tilde{L} \ , \tag{5}$$

where

$$\begin{aligned}
\tilde{W} \otimes \tilde{L} \equiv & \left|1 + C_{V_L}\right|^2 \left(W_{\mu\nu} L^{\mu\nu}\right)_{V_L,V_L} + \left|C_{V_R}\right|^2 \left(W_{\mu\nu} L^{\mu\nu}\right)_{V_R,V_R} + \left|C_{S_L}\right|^2 \left(WL\right)_{S_L,S_L} \\
& + \left|C_{S_R}\right|^2 \left(WL\right)_{S_R,S_R} + \left|C_T\right|^2 \left(W_{\mu\nu\rho\sigma} L^{\mu\nu\rho\sigma}\right)_{T,T} + \mathrm{Re}((1 + C_{V_L}) C_{V_R}^*) \left(W_{\mu\nu} L^{\mu\nu}\right)_{V_L,V_R} \\
& + \mathrm{Re}(C_{S_L} C_{S_R}^*) \left(WL\right)_{S_L,S_R} + \mathrm{Re}(C_{S_L} C_T^*) (W_{\mu\nu} L^{\mu\nu})_{S_L,T} \\
& + \mathrm{Re}(C_{S_R} C_T^*) (W_{\mu\nu} L^{\mu\nu})_{S_R,T} \ .
\end{aligned} \tag{6}$$

We split the contributions into the lepton (L) and hadronic (W) tensors. We define

$$L = \sum_{\text{lepton spin}} \langle 0| J_L^\dagger |\ell\bar{\nu}_\ell\rangle \langle \ell\bar{\nu}_\ell| J_{L'} |0\rangle \ , \tag{7}$$

where we suppressed the Lorenz indices in the leptonic tensor. The indices L and L' can take the values $S_{L,R}, V_{L,R}$ and T with

$$J_{S_{L,R}} = (\bar{\ell} P_L \nu_\ell), \qquad J^\mu_{V_{L,R}} = (\bar{\ell}\gamma^\mu P_L \nu_\ell), \qquad J^{\mu\alpha}_T = (\bar{\ell}\sigma^{\mu\alpha} P_L \nu_\ell). \tag{8}$$

We define the hadronic tensor in the following way:

$$W = \sum_{X_c} \frac{1}{2m_B} (2\pi)^3 \langle \bar{B}| J_H^\dagger |X_c\rangle \langle X_c| J_{H'} |\bar{B}\rangle \delta^{(4)}(p_B - q - p_{X_c}) \ , \tag{9}$$

where p_{X_c} is the total momentum of the X_c state and also in this case we suppressed the Lorenz indices. In the presence of NP interactions, the index H and H' can take the values $S_{L,R}, V_{L,R}$ and T where

$$J_{S_{L(R)}} = (\bar{c} P_{L(R)} b) \ , \qquad J^\mu_{V_{L(R)}} = (\bar{c}\gamma^\mu P_{L(R)} b) \ , \qquad J^{\mu\alpha}_T = (\bar{c}\sigma^{\mu\alpha} P_L b) \ . \tag{10}$$

In Eq. (6) we neglected combinations of the form $\left(W_\mu L^\mu\right)_{V_{L(R)},S_{L(R)}}$ and $\left(W_{\mu\rho\sigma} L^{\mu\rho\sigma}\right)_{V_{L(R)},T}$ since they do not contribute in the limit $m_\ell \to 0$ considered in this work. The hadronic tensors W can now be calculated using the heavy quark expansion (HQE) (see e.g. [21]), expressing them in pertubatively calculable coefficients and hadronic matrix elements scaling with inverse powers of m_b. The number of matrix elements proliferates at each higher order in $1/m_b$ (see [22–24]). Here we only consider terms up to $1/m_b^3$ defined as: (see e.g. [25])

$$\begin{aligned}
2m_B \left(\mu_\pi^2\right)^\perp &\equiv -\langle B|\bar{b}_v (iD_\rho)(iD_\sigma) b_v |B\rangle \Pi^{\rho\sigma} \ , \\
2m_B \left(\mu_G^2\right)^\perp &\equiv \frac{1}{2} \langle B|\bar{b}_v \left[iD_\rho, iD_\lambda\right] (-i\sigma_{\alpha\beta}) b_v |B\rangle \Pi^{\alpha\rho} \Pi^{\beta\lambda},
\end{aligned}$$

$$2m_B\,(\rho_D^3)^\perp \equiv \frac{1}{2}\langle B|\bar{b}_v\,[iD_\rho,[iD_\sigma,iD_\lambda]]\,b_v|B\rangle\Pi^{\rho\lambda}v^\sigma,$$

$$2m_B\,(\rho_{LS}^3)^\perp \equiv \frac{1}{2}\langle B|\bar{b}_v\,\{iD_\rho,[iD_\sigma,iD_\lambda]\}\,(-i\sigma_{\alpha\beta})b_v|B\rangle\Pi^{\alpha\rho}\Pi^{\beta\lambda}v^\sigma\,, \tag{11}$$

where $v^\mu = p_B^\mu/m_B$ is the velocity of the B meson and

$$\Pi_{\mu\nu} = g_{\mu\nu} - v_\mu v_\nu\ . \tag{12}$$

In the following, we drop the "perp" superscript for simplicity. Alternative, the HQE parameters can be defined with the full covariant derivative, related to the spatial component via $iD^\mu = v^\mu(iv\cdot D) + D_\perp^\mu$. These definitions were used in Refs. [2, 23, 24] as, in the reparametrization invariant (RPI) basis, it is beneficial to use the full derivative (see discussion in Appendix A of [24] for the relation between these two bases). In principle, the $1/m_b^4$ terms can be included as recently done for the q^2 moment analysis [2]. The two $1/m_b^4$ parameter extracted were found to be consistent with zero. These higher-order corrections were also studied in [26] using the lowest-lying state approximation. Therefore, for this study of NP effects, we only consider terms up to $1/m_b^3$.

2.1 Next-to-leading order corrections

Besides these power-corrections, we also compute the NLO corrections to the triple differential rate for the full NP operator basis in (1). For scalar NP interactions, the NLO corrections to the q^2 spectrum are already given in [27], using results from [28]. The NLO corrections for the SM are well known for both the massive and massless leptons in the semileptonic decay $b\to c\ell\bar{\nu}_\ell$ [29–34].

We compute the $\mathcal{O}(\alpha_s)$ for the structure functions of the hadronic tensor W for the different currents which enter the fully differential decay width. We note that it turns out to be more convenient to express the triple differential rate with respect to $u \equiv p_{X_c}^2 - m_c^2$ instead of E_ν as in [33]. We then extract the predictions for the various moments and forward-backward asymmetries with arbitrary cuts via numerical integration of the differential rate over the allowed phase space, following the approach described in [35].

In general we can express the structure functions as:

$$W_{HH'}(q^2,(v\cdot q)) = W_{HH'}^{(0)}(q^2,(v\cdot q)) + \frac{\alpha_s(\mu)}{\pi}\Big[W_{HH',\text{virt}}^{(1)}(q^2,(v\cdot q)) + W_{HH',\text{real}}^{(1)}(q^2,(v\cdot q))\Big]\,, \tag{13}$$

where "virt" and "real" stand for virtual and real contributions, respectively. The indices HH' run over all possible pairs of NP interactions, e.g. V_LV_R, S_LS_R, etc.

For the ultraviolet and infrared divergences, we use dimensional regularization and define $\epsilon = (4-d)/2$, where d is the space-time dimensions. For the calculation we use the Mathematica package `FeynCalc` [36]. The ultraviolet divergences in the one-loop virtual diagrams are removed by using on-shell quark mass and wave function renormalization. Furthermore, there are additional ultraviolet divergences for the scalar and tensor currents.

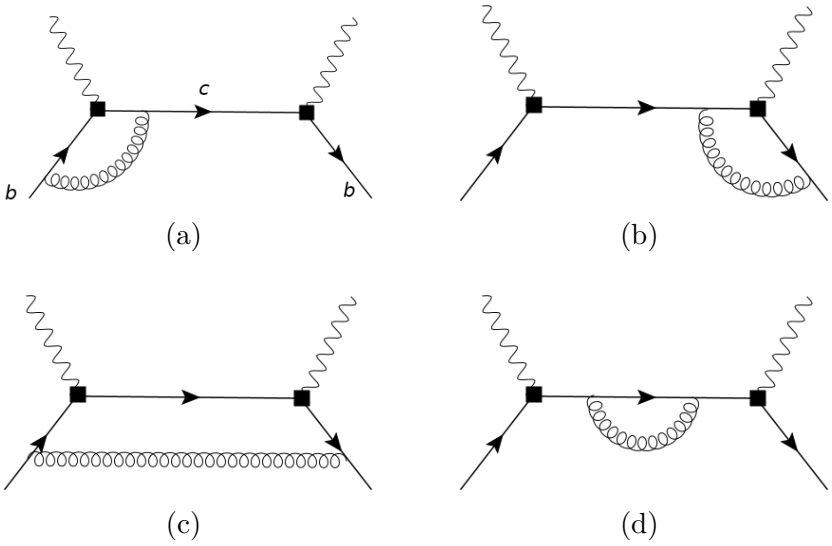

Figure 1: One-loop forward scattering diagrams which contribute to the $b \to X_c \ell \bar{\nu}_\ell$ differential rate at NLO. The black boxes represents one of the currents J_H defined in (10). Solid lines represent the quarks, curly lines the gluons and wavy lines the color-singlet external current mediating the weak decay.

We therefore apply a renormalization of these currents according to their one-loop anomalous dimension (see e.g. [37]). For the computation of real emission we employed the inverse unitarity approach [38]. This method allows us to rewrite the real emission diagram integrated over the gluon phase-space as a multi-loop integral with cut propagators. We can then apply the usual IBP reduction to reduce the real emission contribution to phase-space master integrals which are then calculated explicitly. In the process of the reduction to master integrals we take into account the cut in the gluon and charm intermediate state. For the real emission we encounter the following integral family:

$$I(a,b,c) = \left(4\pi\, e^{-\gamma_E}\right)^{-\epsilon} \text{Disc} \int \frac{\mathrm{d}^d k}{(2\pi)^d} \frac{1}{[k^2]^a [(p_b-k)^2 - m_b^2]^b [(p_b-q-k)^2 - m_c^2]^c} \tag{14}$$

By applying the Cutkosky's rules for the gluon and charm intermediate state:

$$\begin{aligned} \frac{1}{k^2} &\to (-2\pi i)\, \delta(k^2)\,, \\ \frac{1}{(p_b-q-k)^2 - m_c^2} &\to (-2\pi i)\, \delta((p_b-q-k)^2 - m_c^2)\,, \end{aligned} \tag{15}$$

we obtain the following master integrals:

$$\begin{aligned} I(1,0,1) &= \left(4\pi\, e^{-\gamma_E}\right)^{-\epsilon} \int \frac{\mathrm{d}^d k}{(2\pi)^d} (-2\pi i)^2 \delta(k^2) \delta((p_b-q-k)^2 - m_c^2) \Theta(k_0) \\ &= -\frac{\hat{u}}{4\pi \hat{s}} \left(\frac{\hat{u}}{\sqrt{\hat{s}}}\right)^{-2\epsilon} \left(\frac{1}{2} + \epsilon + \mathcal{O}(\epsilon^2)\right)\,, \end{aligned} \tag{16}$$

$$
\begin{aligned}
I(1,1,1) &= \left(4\pi\, e^{-\gamma_E}\right)^{-\epsilon} \int \frac{\mathrm{d}^d k}{(2\pi)^d}\, \frac{1}{(p_b+k)^2 - m_b^2} (-2\pi i)^2 \delta(k^2)\delta((p_b - q - k)^2 - m_c^2)\Theta(k_0) \\
&= \left(\frac{\hat{u}}{\sqrt{\hat{s}}}\right)^{-2\epsilon} \left\{ \frac{1}{8\pi\sqrt{\lambda}} \log\left(\frac{1-\hat{q}^2+\hat{s}+\sqrt{\lambda}}{1-\hat{q}^2+\hat{s}-\sqrt{\lambda}}\right) \right. \\
&\left. + \frac{\epsilon}{4\pi\sqrt{\lambda}} \left[\mathrm{Li}_2\left(\frac{2\sqrt{\lambda}}{1-\hat{q}^2+\hat{s}+\sqrt{\lambda}}\right) + \frac{1}{4}\log^2\left(\frac{1-\hat{q}^2+\hat{s}+\sqrt{\lambda}}{1-\hat{q}^2+\hat{s}-\sqrt{\lambda}}\right)\right] + \mathcal{O}(\epsilon^2) \right\},
\end{aligned}
\tag{17}
$$

where $\hat{s} = \rho + \hat{u}$, $\lambda = \lambda(1, \hat{q}^2, \hat{s})$ and $\lambda(x,y,z) = x^2 + y^2 + z^2 - 2xy - 2xz - 2yz$ is the Källen function. The singularities of the real emissions are located at $\hat{u} = 0$ with:

$$
\hat{u} = (1-\hat{q})^2 - \rho\,, \qquad 0 \le \hat{u} \le \hat{u}_{\max} = (1-\sqrt{\hat{q}^2})^2 - \rho\,. \tag{18}
$$

We have to extract the singular behavior of the master integrals around $\hat{u} = 0$ before expanding in ϵ. The infrared divergences are extracted explicitly by using the plus distribution:

$$
\hat{u}^{-1+a\epsilon} = \frac{1}{a\epsilon}\delta(\hat{u})\,\hat{u}_{\max} + \left[\frac{1}{\hat{u}}\right]_+ + \mathcal{O}(\epsilon)\,. \tag{19}
$$

The integration of the plus distribution over a test function is defined as:

$$
\int_0^{\hat{u}_{\max}} f(\hat{u}) \left[\frac{1}{\hat{u}}\right]_+ \mathrm{d}\hat{u} = \int_0^{\hat{u}_{\max}} \frac{f(\hat{u}) - f(0)}{\hat{u}} \mathrm{d}\hat{u}\,. \tag{20}
$$

In the sum between real and virtual corrections all the infrared divergences cancel. For the γ_5 definition in dimensional regularization we use the Larin prescription [39], i.e.

$$
\gamma_5 = \frac{i}{12}\epsilon_{\mu_1\mu_2\mu_3\mu_4}\gamma^{\mu_1}\gamma^{\mu_2}\gamma^{\mu_3}\gamma^{\mu_4}, \tag{21}
$$

which requires an additional finite renormalization constant in order to restore the correct Ward identity.

Note that, our method to compute the one-loop diagrams differs from [33] where they regularize IR divergences via a finite gluon mass. Ref. [33] presented also the corrections of $\mathcal{O}(\alpha_s^n \beta_0^{n-1})$ (the so-called large-β_0 limit). This can be also done in our approach, however, we do not include them in this analysis. To summarize, in this work we consider leading order, power-corrections up to $\mathcal{O}(1/m_b^3)$ and next-to-leading order corrections. Schematically:

$$
\frac{\mathrm{d}\Gamma_{\mathrm{SM+NP}}}{\mathrm{d}E_\ell \mathrm{d}q^2 \mathrm{d}E_\nu} = \frac{\mathrm{d}\Gamma^{\mathrm{LO}}_{\mathrm{SM+NP}}}{\mathrm{d}E_\ell \mathrm{d}q^2 \mathrm{d}E_\nu} + \frac{\mathrm{d}\Gamma^{\mathrm{Pow}}_{\mathrm{SM+NP}}}{\mathrm{d}E_\ell \mathrm{d}q^2 \mathrm{d}E_\nu} + \left(\frac{\alpha_s}{\pi}\right) \frac{\mathrm{d}\Gamma^{\mathrm{NLO}}_{\mathrm{SM+NP}}}{\mathrm{d}E_\ell \mathrm{d}q^2 \mathrm{d}E_\nu}\,. \tag{22}
$$

2.2 Moments of the spectrum

In the following, we consider the lepton energy moments, dilepton invariant mass (q^2) moments and hadronic invariant mass moments of the $b \to c$ spectrum. The first two can be easily obtained from the triple differential rate defined as in (5). The hadronic invariant mass is related to these variables via

$$M_X^2 \equiv (p_B - q)^2 = (m_B^2 + q^2 - 2m_B(v \cdot q)) \ . \tag{23}$$

The normalized moments for observable $\mathcal{M}$ are then defined

$$\langle \mathcal{M}^n \rangle_{E_\ell > E_\ell^{\rm cut}} = \frac{\int_{E_\ell > E_\ell^{\rm cut}} {\rm d}\mathcal{M}\, \mathcal{M}^n \frac{{\rm d}\Gamma}{{\rm d}\mathcal{M}}}{\int_{E_\ell > E_\ell^{\rm cut}} {\rm d}\mathcal{M}\, \frac{{\rm d}\Gamma}{{\rm d}\mathcal{M}}}, \tag{24}$$

where $E_\ell^{\rm cut}$ is the energy cut of the lepton $\ell = (e, \mu)$ and n denotes the n-th order of moment. Similarly, for q^2 moments, we consider moments with minimum cut $q^2_{\rm cut}$ on the value of q^2. As is customary, we also calculate central moments defined as

$$\langle (\mathcal{M} - \langle \mathcal{M} \rangle)^n \rangle = \sum_{i=0}^{n} \begin{pmatrix} n \\ i \end{pmatrix} \langle (\mathcal{M})^i \rangle \, (- \langle \mathcal{M} \rangle)^{n-i} \, . \tag{25}$$

The moments can be obtained using Eq. (24) and by integrating the triple differential rate over the allowed phase space.

3 New physics in moments of $B \to X_c \ell \bar{\nu}_\ell$

The moments can now be obtained from the triple differential rate in (5). We write

$$\begin{aligned} \langle \mathcal{M} \rangle = \xi_{\rm SM} &+ |C_{V_R}|^2 \, \xi_{\rm NP}^{\langle V_R, V_R \rangle} + |C_{S_L}|^2 \, \xi_{\rm NP}^{\langle S_L, S_L \rangle} + |C_{S_R}|^2 \, \xi_{\rm NP}^{\langle S_R, S_R \rangle} + |C_T|^2 \, \xi_{\rm NP}^{\langle T, T \rangle} \\ &+ {\rm Re}((C_{V_L} - 1) C_{V_R}^*) \, \xi_{\rm NP}^{\langle V_L, V_R \rangle} + {\rm Re}(C_{S_L} C_{S_R}^*) \, \xi_{\rm NP}^{\langle S_L, S_R \rangle} + {\rm Re}(C_{S_L} C_T^*) \, \xi_{\rm NP}^{\langle S_L, T \rangle} \\ &+ {\rm Re}(C_{S_R} C_T^*) \, \xi_{\rm NP}^{\langle S_R, T \rangle} \ , \end{aligned} \tag{26}$$

where we assume that the NP Wilson coefficients are smaller than one so that we can expand the ratios in Eq. (24) up to quadratic NP couplings. The contribution $C_{V_L} \xi_{\rm NP}^{\langle V_L \rangle}$ drops out for normalized moments and in the branching ratio it is equivalent to a rescaling of V_{cb}. The coefficients denoted by ξ depend on the bottom and charm quark masses, the HQE parameters and the lepton energy cut or the q^2 cut. For $\xi_{\rm SM}$, we agree with the numerical results at $\mathcal{O}(\alpha_s)$ given in [40] for the electron energy and M_X moments. The NP coefficients with NLO corrections are lengthy and require numerical integration depending on the lepton energy (or q^2) cut. Therefore, we do not report explicitly our results. They can be obtained in Mathematica format from the authors. However, to illustrate the effect of the NP contributions, we report our predictions for the various central moments for

$m_b^{\rm kin}$	(4.573 ± 0.012) GeV
$\overline{m}_c(2\ {\rm GeV})$	(1.092 ± 0.008) GeV
$(\mu_\pi^2(\mu))_{\rm kin}$	(0.477 ± 0.056) GeV^2
$(\mu_G^2(\mu))_{\rm kin}$	(0.306 ± 0.050) GeV^2
$(\rho_D^3(\mu))_{\rm kin}$	(0.185 ± 0.031) GeV^3
$(\rho_{LS}^3(\mu))_{\rm kin}$	(-0.130 ± 0.092) GeV^3

Table 1: Numerical inputs from [1]. The HQE parameters and the b-quark mass are given in the kinetic scheme at $\mu = 1$ GeV.

benchmark values of the cuts. We consider $E_\ell^{\rm cut} = 1$ GeV in case of the lepton energy and hadronic invariant mass moments. For the q^2 moments, we present results for $q^2_{\rm cut} = 4$ GeV^2. In the next section, we also illustrate the lepton energy or q^2 cut dependence for specific NP scenarios.

In Appendix B we report our predictions for the different moments. We work in the kinetic scheme [28,41–43]. We fix the value of the scale μ in $m_b^{\rm kin}(\mu)$ at 1 GeV. For the charm quark mass we use the $\overline{\rm MS}$ scheme and fix $\overline{m}_c(2\ {\rm GeV})$. For the strong coupling constant we use $\alpha_s(m_b^{\rm kin}) = 0.2184$ [44]. In addition, we use the input values in Table 1. These are obtained from a global fit to lepton energy and hadronic invariant mass moments of the $B \to X_c \ell \bar{\nu}_\ell$ spectra in [1] (which updates the fit of [26]). Interestingly, the value of ρ_D^3 in Table 1 differs from the determination of $\rho_D^3 = (0.03 \pm 0.02)$ GeV^3 found in [2]. The latter uses q^2 moments, which depend on a reduced RPI basis of HQE elements. Specifically, ρ_{LS}^3 does not enter into the prediction of RPI quantities and the dependence on μ_π^2 is very much reduced for normalized q^2 moments. The difference between the values for ρ_D^3 obtained from these two data sets requires further study, preferably via a combined fit to all available data. These studies are in progress. On the contrary, the lepton and hadronic mass moments depends on ρ_{LS}^3 and μ_π^2, so we cannot use the HQE parameter values from [2] for these moments. However, for the q^2 moments both determinations of HQE parameters can be used. We comment on this in the next section.

Our results in Appendix B show the impact of different NP contributions. As stated already in the introduction, especially for the M_X and q^2 moments, the inclusion of $1/m_b$ power corrections is crucial, while in addition for the former also α_s numerically plays an important role. In principle, the coefficients have an uncertainty stemming from the input parameters. However, here we refrain from giving those. We include them in the next section when discussing different NP scenarios.

From our results, we observe that for all moments the contribution proportional to C_T^2 is sizable compared to $\xi_{\rm SM}$. Especially for the third E_ℓ and q^2 moments, tensor contributions can be as large as ten times the SM prediction or more (for order one coefficients). Therefore, a moment analysis is expected to be able to strongly constrain such contributions. It is also interesting to consider the case of contributions from both C_{S_L} and C_T, because due

to RGE running (see e.g. [45, 46]), tensor interactions always generate left-handed scalar interactions. We note that q^2 moments are only sensitive to the quadratic contributions, while lepton and hadronic mass moments are also sensitive to interference. Assuming real couplings and $C_{S_L} > C_T$ (see discussion in [11]), we observe that the q^2 moments mainly constrain C_{S_L}, while the lepton moments constrain the tensor part. Clearly, the situation for the inclusive decay is not as straightforward as for the exclusive case, because our current "SM prediction" depends on the input of the HQE elements that are extracted from data. Nevertheless, we can visualize and investigate the potential NP bounds for different scenarios by assuming that the SM prediction is known (namely $\xi_{\rm SM}$). We then define

$$\delta\langle\mathcal{M}\rangle \equiv \frac{\langle\mathcal{M}\rangle - \langle\mathcal{M}\rangle_{\rm SM}}{\langle\mathcal{M}\rangle_{\rm SM}} \tag{27}$$

where $\mathcal{M}_{\rm SM} = \xi_{\rm SM}$ for the specific moment under consideration. Considering then a 10% measurement of the moments, i.e. $\delta\langle\mathcal{M}\rangle = \pm 0.1$, leads to a constraint on the NP parameters. Specifically, for the $S_L - T$ contributions we obtain

$$-0.1 < |C_{S_L}|^2 \hat{\xi}_{\rm NP}^{\langle S_L, S_L\rangle} + |C_T|^2 \hat{\xi}_{\rm NP}^{\langle T,T\rangle} + {\rm Re}(C_{S_L} C_T^*) \hat{\xi}_{\rm NP}^{\langle S_L, T\rangle} < 0.1 \ , \tag{28}$$

where

$$\hat{\xi}_i \equiv \frac{\xi_i}{\xi_{\rm SM}} \ , \tag{29}$$

and the ξ_i can be found in Appendix B for the different moments and NP scenarios. In order to illustrate the effects, we use these ξ's, which are re-expanded in the Wilson coefficients. The constraints obtained from (28) are illustrated in Fig. 2. Interestingly, we see that the different moments give complementary bounds on NP, similar as the $B \to D$ versus $B \to D^*$ constraints in the exclusive case (for the latter see [11]).

Similarly, in Fig. 3, we illustrate the possible bounds on C_{V_L} and C_{V_R} (left) and C_{S_L} and C_{S_R} (right). In these cases, we see that the M_X moments give much weaker constraints than the lepton energy and q^2 moments. We should stress that the uncertainties on the M_X moments are in general also larger as they are more sensitive to higher-order HQE corrections. Comparing with the exclusive constraints on C_{S_L} versus C_{S_R} in [11], we observe that such a SM measurement would constrain NP along the $C_{S_L} = -C_{S_R}$ plane, similar as the $B \to D$ exclusive mode, while $B \to D^*$ gives constraints orthogonal to that.

Finally, we note that the $C_{S_{L,R}} C_T$ coefficient vanishes for q^2 moments because the differential rate has only a parity-odd contribution while q^2 moments with a cut on q^2 are parity even observables. For lepton energy and hadronic mass moments, the contribution proportional to $C_{S_R} C_T$ is non-zero only due to power corrections. Therefore, the sensitivity to these types of NP is limited.

3.1 Illustration for specific NP scenarios

To visualize the effect of possible NP in the moments of the $B \to X_c \ell \bar{\nu}_\ell$ spectrum as a function of the lepton energy cut (or q^2 cut), we consider three NP scenarios specified

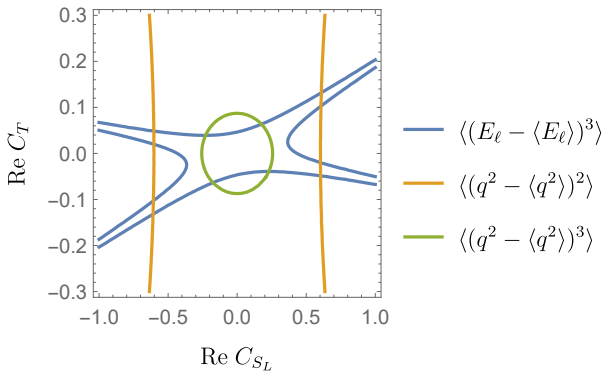

Figure 2: Illustration of complementarity of constraints on C_{S_L} and C_T from lepton energy moments and q^2 moments, assuming $\delta\langle\mathcal{M}\rangle = \pm 0.1$.

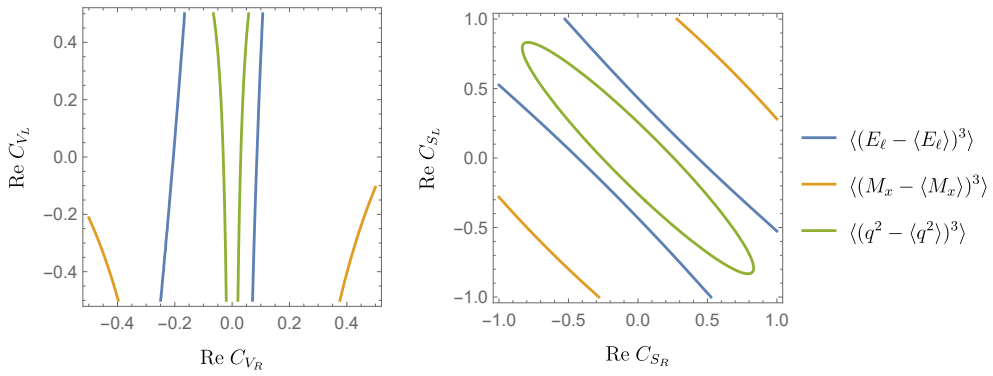

Figure 3: Illustration of the possible bounds on (left) C_{V_L} versus C_{V_R} and (right) C_{S_L} versus C_{S_R} assuming a 10% SM measurement.

in Table 2 allowing for either new scalar interactions (Scen. I), new tensor and scalar interactions interactions (Scen. II) and new vector interactions (Scen. III). These scenarios are just to illustrate how the NP contributions depend on the cut and to the SM uncertainty. We stress that these scenarios may not be realistic in light of current data on exclusive $B \to D^{(*)}$ decays, were the same NP operators would contribute. Specifically Scenario II, where we allow for a rather large tensor contribution, may be already excluded by the exclusive decays (see [11]). For the scalar contributions, we pick $C_{S_R} = C_{S_L}$, based on Fig. 3 as we see that this would give a large effect on the spectrum. Finally, as here we consider rather large Wilson coefficients we do not re-expand the expression for the moments in the Wilson coefficients. We observe in Figs. 4, 5 and 6 that the prediction for all central moments are modified by the presence of NP contributions, but that the cut-dependence remains similar as that of the SM prediction. For all cases, we observe that the third central moment is most sensitive to NP effects.

NP Scenarios	C_{V_L}	C_{V_R}	C_{S_R}	C_{S_L}	C_T
I	0	0	1	1	0
II	0	0	0	-1	0.5
III	1	0.5	0	0	0

Table 2: Three NP scenarios that we consider to visualize the effect of the NP parameters in the moments. All Wilson coefficients are defined at the scale $\mu = m_b$.

Electron energy moments:

Figure 4 shows the lepton energy moments as a function of the lepton energy cut for the SM and the three NP scenarios. In order to qualitatively understand the sensitivity on possible NP effects, we show in these plots the experimental results from Belle [47] and BaBar [48]. On the right-hand side, we show the impact of the NP scenarios by showing the absolute value of $\delta \langle \mathcal{M} \rangle$ defined in (27).

For simplicity, we only show an uncertainty band for the SM prediction obtained by varying the inputs in Table 1 within their 1σ ranges. To account for missing α_s corrections, we vary the scale of $\alpha_s(\mu)$ in the range $m_b/2 < \mu < 2\, m_b$. We observe for electron energy moments, Scen. I is rather close to the SM, while Scen. II and III cause a shift much larger than the SM uncertainty. These lepton energy moments therefore seem rather sensitive to NP effects and it would be potentially able to constrain NP via a full global analysis of these moments. Note also that the contribution from power corrections are in general small for this kind of moments, reducing the dependence on the value of the HQE parameters.

M_X^2 moments:

Results for the hadronic invariant mass moments are shown in Fig. 5. We observe that these moments are sensitive to new scalar couplings, as Scen. I shows the largest deviation from the SM prediction. On the other hand, both Scen. II and III lie within the uncertainty of the SM error band, which is rather large. This happens because for the M_X moments the contribution from power corrections is very important and the α_s corrections are much larger compared to the partonic LO. The dependence of the M_X moments on the scale of α_s is therefore much larger compared for instance to the electron energy moments and so prevents a precise SM determination of these kind of observables.

For the experimental data points we use the results of CLEO [49], Belle [50] and BaBar [51]. The latter does not provide the central moments but only $\langle (M_X^2)^{i=1,2,3} \rangle$. We have calculated the central moments using (25). We do not show the recent results of Belle II [52] since the uncertainties are still rather large.

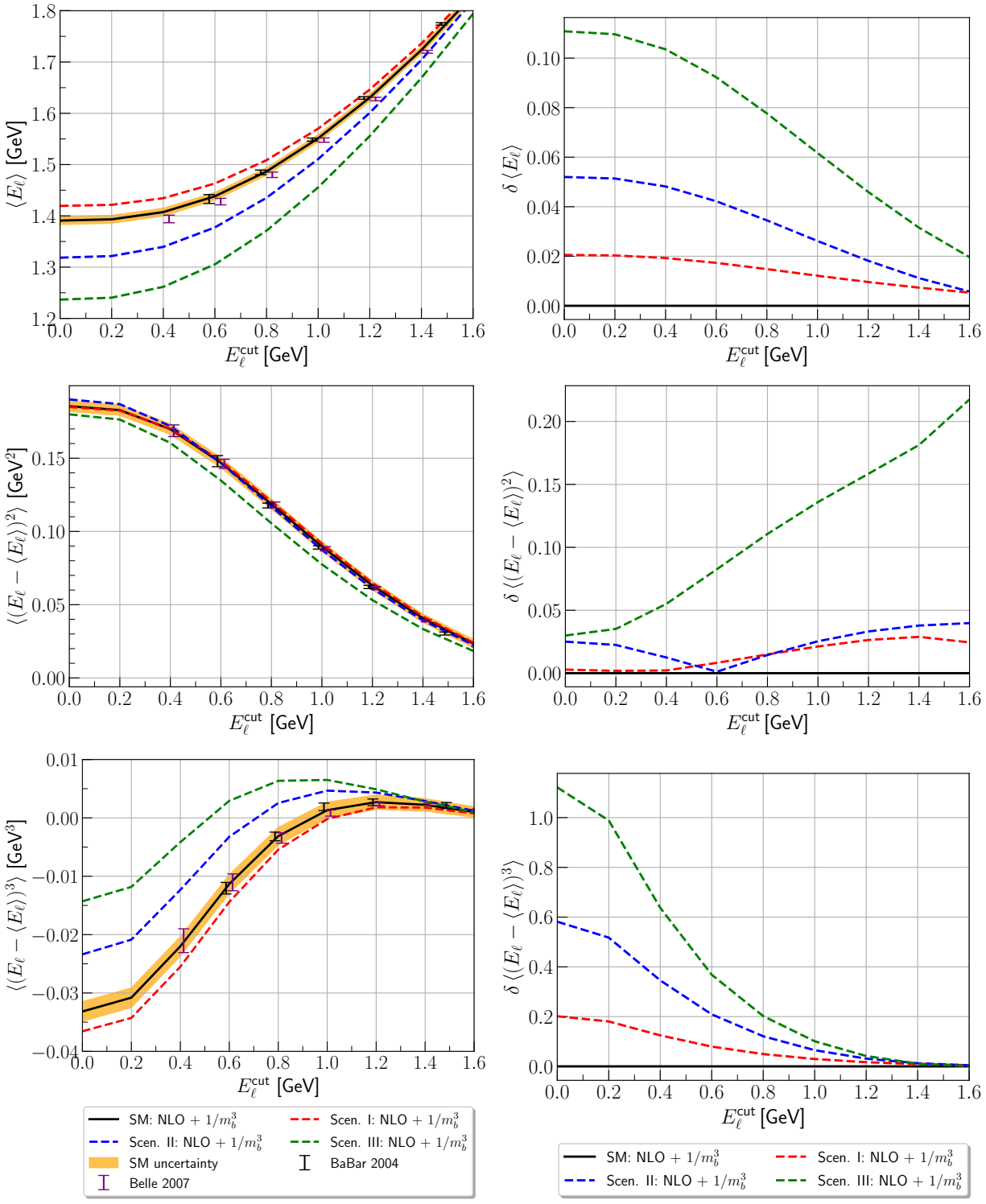

Figure 4: Lepton energy moments for the $B \to X_c \ell \bar{\nu}_\ell$ decay for the different NP scenarios (see Tab. 2). The experimental results of BaBar is taken from [48] and Belle from [47].

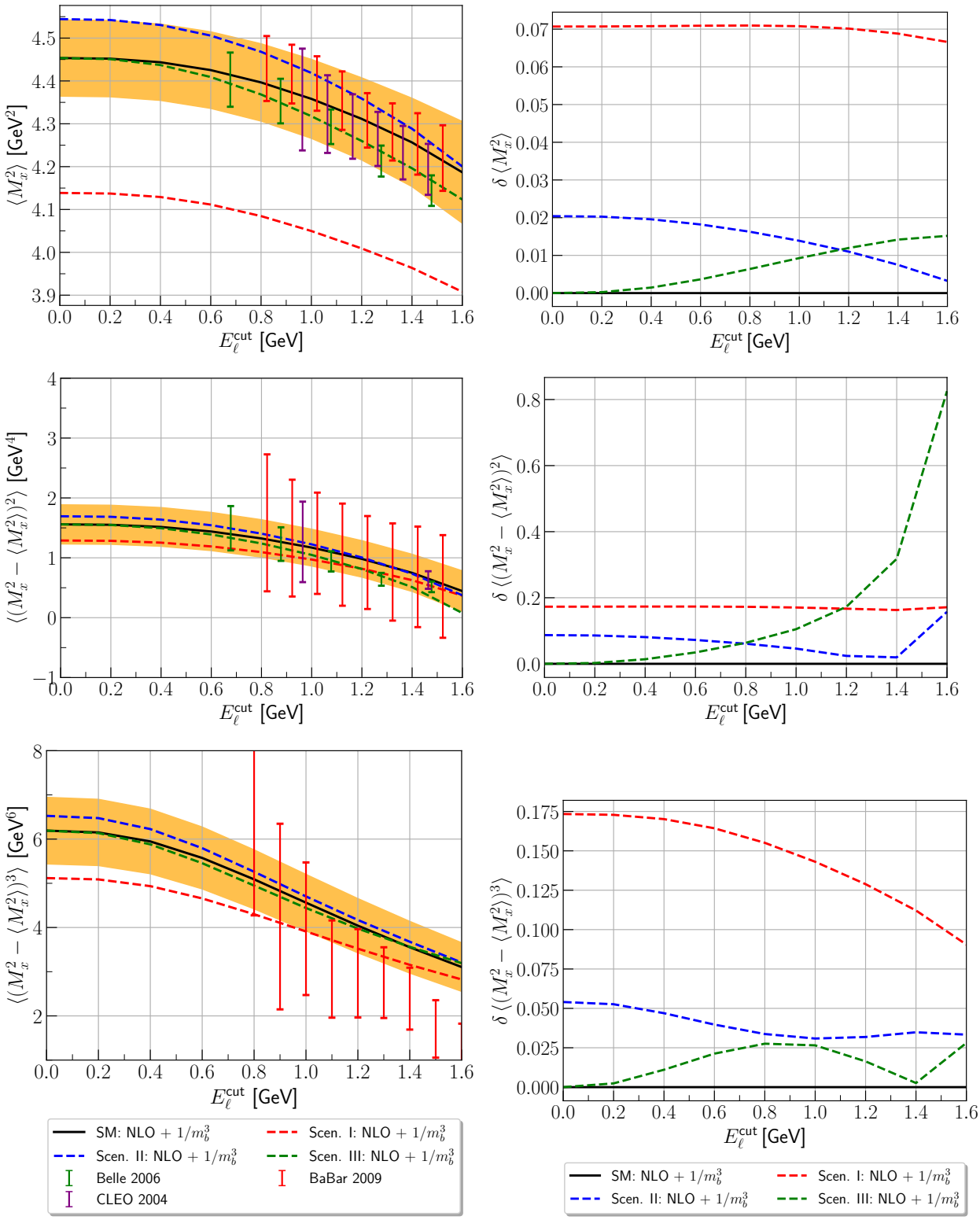

Figure 5: Hadronic invariant mass moments for the $B \to X_c \ell \bar{\nu}_\ell$ decay different NP scenarios (see Tab. 2). The experimental values of BaBar is taken from [51], CLEO [49], Belle [50].

	$\mathcal{B}(B \to X_c \ell \bar{\nu})$ in %
$\xi_{\rm SM}$	$12.983\vert_{\rm LO} - 0.962\vert_{\rm pow} - \left(\frac{\alpha_s}{\pi}\right) 16.101$
$\xi_{\rm NP}^{\langle V_R, V_R\rangle}$	$12.983\vert_{\rm LO} - 0.962\vert_{\rm pow} - \left(\frac{\alpha_s}{\pi}\right) 16.101$
$\xi_{\rm NP}^{\langle S_L, S_L\rangle}$	$3.245\vert_{\rm LO} + 0.067\vert_{\rm pow} + \left(\frac{\alpha_s}{\pi}\right) 2.783$
$\xi_{\rm NP}^{\langle S_R, S_R\rangle}$	$3.245\vert_{\rm LO} + 0.067\vert_{\rm pow} + \left(\frac{\alpha_s}{\pi}\right) 2.783$
$\xi_{\rm NP}^{\langle T, T\rangle}$	$155.802\vert_{\rm LO} - 16.493\vert_{\rm pow} - \left(\frac{\alpha_s}{\pi}\right) 163.665$
$\xi_{\rm NP}^{\langle V_L, V_R\rangle}$	$-8.453\vert_{\rm LO} + 1.332\vert_{\rm pow} + \left(\frac{\alpha_s}{\pi}\right) 13.375$
$\xi_{\rm NP}^{\langle S_L, S_R\rangle}$	$4.226\vert_{\rm LO} + 0.380\vert_{\rm pow} + \left(\frac{\alpha_s}{\pi}\right) 4.550$
$\xi_{\rm NP}^{\langle S_L, T\rangle}$	0
$\xi_{\rm NP}^{\langle S_R, T\rangle}$	0

Table 3: Numerical values of the parameters for the branching ratio without lepton energy cut for fixed B meson lifetime.

q^2 moments:

For the q^2 moments, we consider the SM and NP predictions at different values of the q^2 cut shown in Figure 6. For the plots on the left-hand side, we used the HQE parameters from Table 1 from [1]. Comparing with the experimental data points of Belle [53] and Belle II [54], we find large deviations. Interestingly, these deviations cannot be accommodated by the three NP scenarios we consider. As mentioned before, in [2], where these data were used to extract the HQE parameters and V_{cb}, a value of ρ_D^3 incompatible with that in Table 1 was found. The mismatch in Fig. 6 is a consequence of this: the q^2 data pull ρ_D^3 to much smaller value. To illustrate this, we show on the right-hand side of Fig. 6 the SM predictions using the HQE parameters obtained in [2]. We observe good agreement with the data points. In addition, the uncertainty of the SM prediction is rather large, reflecting that these moments are more sensitive to the power corrections than the lepton energy moments. This was already observed in [55]. Note that the ξ coefficients in Appendix B are obtained using Table 1. As the goal of these scenarios is merely to demonstrate the effect of different NP parameters, we do not present ξ's using the HQE parameters from [2]. We observed the q^2 moments are most sensitive to Scen. I, while Scen. III has basically no effect. This is because for this scenario there is a cancellation between the Wilson coefficients, rendering the effect almost unobservable. For smaller values of C_{V_L}, there is an effect on the moments and in fact the q^2 moments can put rather strong constraints as seen in Fig. 3.

3.2 Lepton Flavor Universality Ratios

In order to study NP in Lepton Flavor Universality Ratios of light leptons, we give the analytic expression for the total rate in Appendix A.

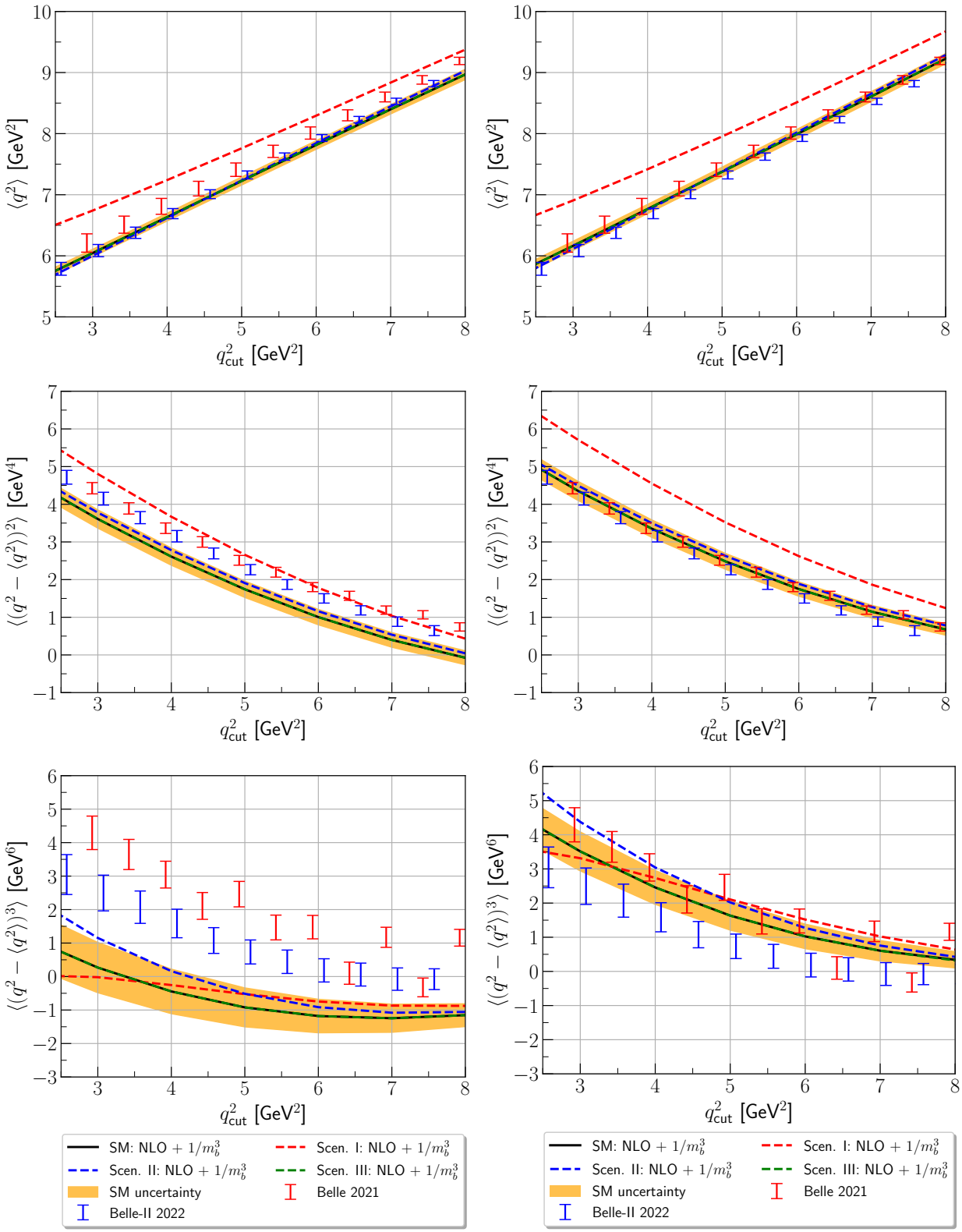

Figure 6: Dilepton invariant mass moments (q^2) for the $B \to X_c \ell \bar{\nu}_\ell$ decay in comparison with Belle [53] and Belle II data [54]. (Left) Using the inputs in Table 1 from [1](Right) using the inputs from [2].

For completeness, we also give the numerical coefficients including NLO correction. Writing the branching ratio in terms of ξ_i as in (26), with the only difference that the $\xi_{\rm SM}$ term gets multiplied with $|1 + C_{V_L}|^2$, we find the coefficients listed in Table 3. We used the iputs in Table 1 and a fixed value for the B meson lifetime $\tau_B = 1.579$ ps [56] and $|V_{cb}| = (42.16 \pm 0.51) \cdot 10^{-3}$ [1]. However, we note that NP would also affect the total lifetime of the B meson.

The expressions in the Appendix and our numerical results can be used to study ratios of electron versus muon rates under the assumption of lepton-flavour universality violating new physics. Note that a lepton-flavour universal and diagonal NP effect in C_L can in principle be absorbed by a shift in V_{cb}. Recently, the SM predictions for lepton-flavour universality ratios were studied [57]. Because the current data (see for example the q^2 moments split up for electron and muon contributions in [53]) do not indicate any deviation from lepton universality in the charged light modes, we do not study these effects here further.

3.3 HQE parameters versus NP

The HQE parameters are extracted from moments of the $b \to c$ spectrum under the assumption of the SM. However, it can be that NP mimics the effect of the HQE parameters shifting the spectrum up or down. In fact, Fig. 6 shows that shifting ρ_D^3 seems to be able to mimic the effect that NP may have on the spectrum. It would therefore be interesting to perform a full analysis of the moments including NP. Such an analysis lies beyond the scope of the current paper. However, we can illustrate the possible effect with a simplified toy fit. To this extend, we generate pseudo data points for the three NP scenarios in Table 2 for lepton energy and hadronic invariant mass moments at different lepton energy cuts as well as q^2 moments with $q^2_{\rm cut}$. For this, we use the HQE parameters in Table 1. We generate 9 data points per scenario: the first, second and third central moments with $E_\ell^{\rm cut} = 1.0$ GeV for the lepton energy and hadronic invariant mass moments and with $q^2_{\rm cut} = 4$ GeV^2 for q^2 moments. For the uncertainty on these points, we vary the contribution of ρ_D^3 by 30%, μ_G^2 by 20% and α_s between its value at $\mu = m_b/2$ and $\mu = m_b$, based on [1, 2]. As this render the uncertainty for the lepton energy moments rather small, we add an additional uncertainty based on the current experimental uncertainty. In addition, we also include the current experimental uncertainty for the third q^2 and M_X moments as these are rather large.

In principle, these pseudo data points can then be used to fit for the HQE parameters $\mu_G^2, \mu_\pi^2, \rho_{LS}^3, \rho_D^3$ using the SM expressions. In this way, our toy fit mimics a situation that may happen in reality: i.e. NP is present but the extraction of HQE parameters is done assuming the SM. We observe that for the three NP scenarios in Table 2, our simple toy fit yields large χ^2. The reason for this is that it is challenging to accommodate the third moments, which are sensitive to NP, and first lepton energy moments, which drives the fit due to its small uncertainty, at the same time. Turning the argumentation around this may indicate that a full simultaneous fit of the HQE parameters and NP parameters would give rather good constraints on NP. In this endeavour, it seems crucial to improve the experimental inputs especially on the third moments.

Finally, we may also consider a more realistic scenario taken from the analysis of [11]: $C_T = 0.05$ and $C_{S_L} = -0.5$. Assuming no correlations between the pseudo data points, we obtain a $\chi^2/d.o.f. \simeq 2.4$ and

$$\mu_G^2|_{\rm toy} = 0.40\ {\rm GeV}^2,\ \ \mu_\pi^2|_{\rm toy} = 0.45\ {\rm GeV}^2,\ \ \rho_{LS}^3|_{\rm toy} = 0.09\ {\rm GeV}^3,\ \ \rho_D^3|_{\rm toy} = 0.11\ {\rm GeV}^3. \tag{30}$$

Comparing with the values in Table 1, we find $1-2\sigma$ shifts, with a rather poor fit quality. We note that this toy fit merely serves to illustrate how NP could be hidden in the HQE extraction, because the fit is rather flexible in accounting for such variations. Strong conclusions should not be made from this fit, except that it may be worth performing a full analysis on data. On the other hand, we also note that this may be challenging due to the large number of extra parameters.

4 Forward-backward asymmetry

In this section, we consider the forward-backward asymmetry discussed in [15] and more recently in [16]. The asymmetry is defined as

$$A_{FB} \equiv \frac{\displaystyle\int_{-1}^{0} {\rm d}z \frac{{\rm d}\Gamma}{{\rm d}z} - \int_{0}^{1} {\rm d}z \frac{{\rm d}\Gamma}{{\rm d}z}}{\displaystyle\int_{-1}^{1} {\rm d}z \frac{{\rm d}\Gamma}{{\rm d}z}}\ , \tag{31}$$

where

$$z \equiv \cos\theta = \frac{v\cdot p_{\bar\nu_\ell} - v\cdot p_\ell}{\sqrt{(v\cdot q)^2 - q^2}}\ , \tag{32}$$

and θ is the angle between spacial momenta of the lepton and the B meson in the rest-frame of the dilepton pair.

As discussed in [16], including a lepton energy cut $E_\ell^{\rm cut}$ in the A_{FB} definition leads to a cusp in the differential spectrum in the variable z, which can be problematic in experimental analysis. To circumvent this issue, Ref. [16] proposed to study A_{FB} with a minimum cut on q^2 instead of E_ℓ. We therefore consider only q^2 cuts, which also considerably simplifies the calculation. We refer to [16] for details of the calculation.

Writing our results as in (26), we find the ξ's listed in Table 4. We consider for the first time the α_s-corrections, both for the SM and for NP scenarios. In the upper part of Fig. 7, we show the differential distribution in z normalized to $1/\Gamma_0$ as defined in Appendix A for the SM and our three NP scenarios in Table 2. Our normalization, i.e. using only $1/\Gamma_0$, differs from that used by [15, 16], but our results for the SM are in agreement. In the lower panel of Fig. 7, we show the prediction for A_{FB} as a function of $q^2_{\rm cut}$ where we plot the different SM contributions for illustration. The plots shows that forward-backward asymmetry and the differential distribution are sensitive the NP contributions and can distinguish among our three different scenarios. The forward-backward asymmetry has not

been measured so far, but our analysis shows the potential for understanding the SM and possibly to constrain NP contributions.

	$A_{FB} \cdot 10^{-2}$
$\xi_{\rm SM}$	$24.603\vert_{\rm LO} - 2.928\vert_{\rm pow} - \left(\frac{\alpha_s}{\pi}\right) 6.63$
$\xi_{\rm NP}^{\langle V_R, V_R\rangle}$	$-25.387\vert_{\rm LO} + 0.769\vert_{\rm pow} + \left(\frac{\alpha_s}{\pi}\right) 4.47$
$\xi_{\rm NP}^{\langle S_L, S_L\rangle}$	$-8.683\vert_{\rm LO} - 0.333\vert_{\rm pow} - \left(\frac{\alpha_s}{\pi}\right) 15.91$
$\xi_{\rm NP}^{\langle S_R, S_R\rangle}$	$-8.683\vert_{\rm LO} - 0.333\vert_{\rm pow} - \left(\frac{\alpha_s}{\pi}\right) 15.91$
$\xi_{\rm NP}^{\langle T, T\rangle}$	$-254.730\vert_{\rm LO} + 40.911\vert_{\rm pow} + \left(\frac{\alpha_s}{\pi}\right) 2.13$
$\xi_{\rm NP}^{\langle V_L, V_R\rangle}$	$-24.208\vert_{\rm LO} + 4.025\vert_{\rm pow} + \left(\frac{\alpha_s}{\pi}\right) 7.53$
$\xi_{\rm NP}^{\langle S_L, S_R\rangle}$	$12.104\vert_{\rm LO} - 1.415\vert_{\rm pow} - \left(\frac{\alpha_s}{\pi}\right) 24.67$
$\xi_{\rm NP}^{\langle S_L, T\rangle}$	$49.207\vert_{\rm LO} + 0.954\vert_{\rm pow} + \left(\frac{\alpha_s}{\pi}\right) 51.17$
$\xi_{\rm NP}^{\langle S_R, T\rangle}$	$2.20\vert_{\rm pow}$

Table 4: Numerical values of the parameters for the A_{FB} given in Eq. (26). We consider $q^2_{\rm cut} = 4$ GeV^2.

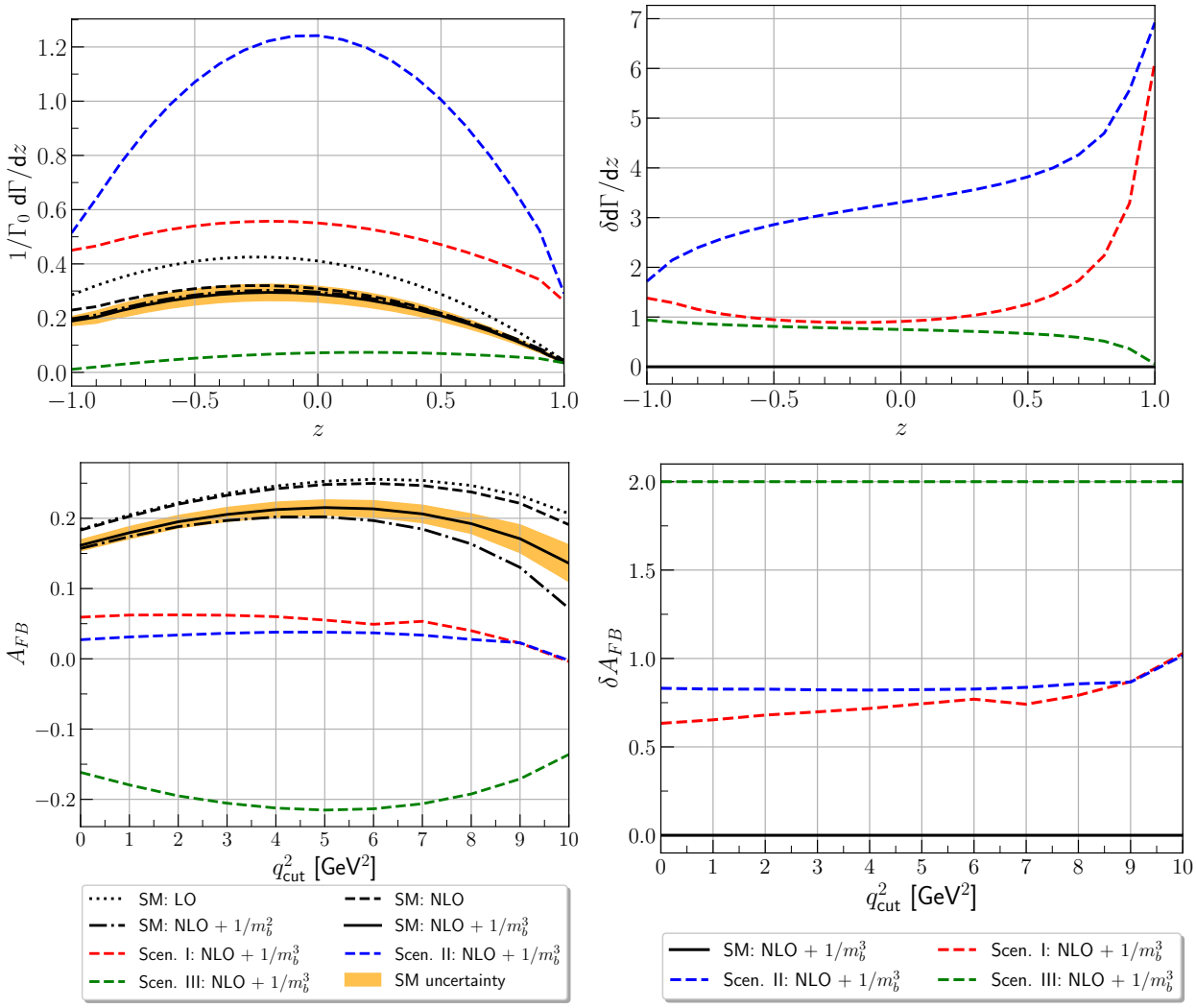

Figure 7: (Upper part) The differential rate for $B \to X_c \ell \bar{\nu}_\ell$ as a function of z without lepton energy cut and relative size of the NP scenarios w.r.t. the SM prediction. (Lower part) Forward-backward asymmetry as a function of the q^2 cut for the three NP scenarios in Table 2 and their relative size w.r.t. the SM.

5 Conclusion

We investigated New Physics effects on the semileptonic channel $B \to X_c \ell \bar{\nu}_\ell$. For the first time, we compute power-corrections up to $\mathcal{O}(1/m_b^3)$ and α_s-corrections for the full basis of the New Physics operators in the WET over the full differential decay width. These corrections are necessary to properly describe the dominant NP contributions to central moments of dilepton invariant mass q^2 and hadronic invariant mass M_X^2.

We compared SM predictions, using HQE parameters obtained from experimental data, and experimental measurements to the moments of lepton energy, hadronic invariant mass

and dilepton momentum for different toy New Physics scenarios. In addition, we also computed the forward-backward asymmetry. The main goal of this work is to pave the way for a global fit analysis, which includes the full base of NP operators. To further constrain such global fit, one may take advantage of lattice results for the HQE parameters, extracted from meson mass calculations at different quark mass values [58], and scattering matrix for $B \to X_c \ell \bar{\nu}_\ell$ [59, 60]. Such results, even if preliminary, could enhance the predictive power of the HQE by better assessing the non-perturbative inputs. We aim to perform such a fit using the EOS software [17].

Acknowledgements

We thank T. Mannel and M. Bordone for discussion and correspondence. This research was supported by the Deutsche Forschungsgemeinschaft (DFG, German Research Foundation) under grant 396021762 - TRR 257.

A NP contributions to the total rate

We decompose the prediction of the total rate in two parts:

$$\Gamma(B \to X_c \ell \bar{\nu}) = \Gamma_0 \left(\Gamma_{\rm NP}^{\rm LO}(B \to X_c \ell \bar{\nu}) + \Gamma_{\rm NP}^{\rm Pow}(B \to X_c \ell \bar{\nu}) \right) \tag{33}$$

where

$$\Gamma_0 = \frac{G_F^2 |V_{cb}|^2 m_b^5}{192 \pi^3} (1 + A_{\rm ew}) \tag{34}$$

and $A_{\rm ew} = 0.014$ [61]. The LO result in the free quark approximation is given by

$$\begin{aligned} \Gamma_{\rm NP}^{\rm LO}(B \to X_c \ell \bar{\nu}) = \Gamma_{\rm SM}^{\rm LO}(B \to X_c \ell \bar{\nu}) \left(|1 + C_{V_L}|^2 + |C_{V_R}|^2 + \frac{1}{4} \left(|C_{S_L}|^2 + |C_{S_R}|^2 \right) + 12 |C_T|^2 \right) \\ + \Gamma_{\rm mix}^{\rm LO}(B \to X_c \ell \bar{\nu}) \left({\rm Re}((1 + C_{V_L}) C_{V_R}) - \frac{1}{2} {\rm Re}(C_{S_L} C_{S_R}) \right) , \end{aligned} \tag{35}$$

with

$$\Gamma_{\rm SM}^{\rm LO} = (1 - 8\rho - 12\rho^2 \log(\rho) + 8\rho^3 - \rho^4) , \tag{36}$$

$$\Gamma_{\rm mix}^{\rm LO} = -4\sqrt{\rho} \, (1 + 9\rho + 6\rho(1 + \rho) \log(\rho) - 9\rho^2 - \rho^3) . \tag{37}$$

Our result agrees with the leading-order (LO) results from [11]. The contribution from the power corrections is

$$\begin{aligned} \Gamma_{\rm NP}^{\rm Pow}(B \to X_c \ell \bar{\nu}) = \frac{\mu_\pi^2}{m_b^2} \Gamma_{\rm SM}^{\mu_\pi^2} \Bigg(|1 + C_{V_L}|^2 + |C_{V_R}|^2 + \frac{1}{4} (|C_{S_L}|^2 + |C_{S_R}|^2) + 12 |C_T|^2 \\ - 2\sqrt{\rho} \big(\rho^3 + 9\rho^2 - 9\rho - 6(\rho + 1)\rho \log(\rho) - 1 \big) \big({\rm Re}((1 + C_{V_L}) C_{V_R}^*) \end{aligned}$$

$$
\begin{aligned}
&-\frac{1}{2}\mathrm{Re}(C_{S_L}C_{S_R}^*)\Big) + \left(\frac{\mu_G^2}{m_b^2} - \frac{\rho_{LS}^3}{m_b^3}\right)\Big(\Gamma_{\rm SM}^{\mu_G^2}\left(|1+C_{V_L}|^2 + |C_{V_R}|^2\right)\\
&-\frac{1}{8}\big(5\rho^4 - 32\rho^3 + 72\rho^2 - 32\rho + 12(\rho-4)\rho\log(\rho) - 13\big)(|C_{S_L}|^2 + |C_{S_R}|^2)\\
&-2\big(15\rho^4 - 64\rho^3 + 24\rho^2 + 12(3\rho+4)\rho\log(\rho) + 25\big)|C_T|^2\\
&+\frac{2\sqrt{\rho}}{3}\big(13\rho^3 - 27\rho^2 - 6(3\rho^2 - 3\rho + 2)\log(\rho) + 27\rho - 13\big)\mathrm{Re}((1+C_{V_L})C_{V_R}^*)\\
&-3\sqrt{\rho}\big(\rho^3 - 3\rho^2 - 2(\rho^2 - 5\rho - 2)\log(\rho) - 9\rho + 11\big)\,\mathrm{Re}(C_{S_L}C_{S_R}^*)\big)\\
&+\frac{\rho_D^3}{m_b^3}\Bigg(\Gamma_{\rm SM}^{\rho_D^3}\left(|1+C_{V_L}|^2 + |C_{V_R}|^2\right) + \frac{1}{24}\big(-5\rho^4 - 8\rho^3 + 12(3\rho^2 + 8\rho + 8)\log(\rho)\\
&-184\rho + 197\big)\left(|C_{S_L}|^2 + |C_{S_R}|^2\right) + 2\big(-5\rho^4 - 8\rho^3 + 32\rho^2 + 4(9\rho^2 - 8\rho + 8)\log(\rho)\\
&-56\rho + 37\big)|C_T|^2 + 2\left(\rho^3 - 15\rho^2 + 6(\rho^2 - \rho - 2)\log(\rho) + 39\rho - 25\right)\\
&\times\mathrm{Re}((1+C_{V_L})C_{V_R}^*) + \frac{2\sqrt{\rho}}{6}\big(\rho^3 + 9\rho^2 + (-18\rho^2 + 90\rho + 60)\log(\rho)\\
&-153\rho + 143\big)\,\mathrm{Re}(C_{S_L}C_{S_R}^*)\big)
\end{aligned}
\tag{38}
$$

with

$$\Gamma_{\rm SM}^{\mu_\pi^2} = -\frac{1}{2}\Gamma_{\rm SM}^{\rm LO}\,, \tag{39}$$

$$\Gamma_{\rm SM}^{\mu_G^2} = -\frac{1}{2}(5\rho^4 - 24\rho^3 + 24\rho^2 + 12\rho^2\log(\rho) - 8\rho + 3)\,, \tag{40}$$

$$\Gamma_{\rm SM}^{\rho_{LS}^3} = \frac{1}{2}\left(5\rho^4 - 24\rho^3 + 24\rho^2 + 12\rho^2\log(\rho) - 8\rho + 3\right)\,, \tag{41}$$

$$\Gamma_{\rm SM}^{\rho_D^3} = \frac{1}{6}\left(-5\rho^4 - 8\rho^3 + 24\rho^2 + 12(3\rho^2+4)\log(\rho) - 88\rho + 77\right)\,. \tag{42}$$

For the power-corrections $\mathcal{O}(1/m_b^2)$ of $(1+C_{V_L})C_{V_R}$ our result agrees with [14] $c_L c_R$ term.

B NP effects on the moments

In this Appendix, we list the coefficients ξ defined in 26. We categorize the contributions of leading-order, power-corrections and α_s corrections.

	$\langle E_\ell \rangle \cdot 10^{-2}$	$\langle (E_\ell - \langle E_\ell \rangle)^2 \rangle \cdot 10^{-2}$	$\langle (E_\ell - \langle E_\ell \rangle)^3 \rangle \cdot 10^{-3}$
$\xi_{\rm SM}$	$157.23\vert_{\rm LO} - 1.78\vert_{\rm pow} - \left(\frac{\alpha_s}{\pi}\right) 4.608$	$8.715\vert_{\rm LO} + 0.291\vert_{\rm pow} - \left(\frac{\alpha_s}{\pi}\right) 1.970$	$-3.076\vert_{\rm LO} + 3.399\vert_{\rm pow} + \left(\frac{\alpha_s}{\pi}\right) 14.388$
$\xi_{\rm NP}^{\langle V_R, V_R\rangle}$	$-10.00\vert_{\rm LO} + 1.63\vert_{\rm pow} + \left(\frac{\alpha_s}{\pi}\right) 1.172$	$0.188\vert_{\rm LO} - 0.242\vert_{\rm pow} + \left(\frac{\alpha_s}{\pi}\right) 0.531$	$9.394\vert_{\rm LO} - 1.555\vert_{\rm pow} - \left(\frac{\alpha_s}{\pi}\right) 5.711$
$\xi_{\rm NP}^{\langle S_L, S_L\rangle}$	$0.849\vert_{\rm pow} + \left(\frac{\alpha_s}{\pi}\right) 0.414$	$0.128\vert_{\rm pow} - \left(\frac{\alpha_s}{\pi}\right) 0.161$	$-0.712\vert_{\rm pow} + \left(\frac{\alpha_s}{\pi}\right) 0.0365$
$\xi_{\rm NP}^{\langle S_R, S_R\rangle}$	$0.849\vert_{\rm pow} + \left(\frac{\alpha_s}{\pi}\right) 0.414$	$0.128\vert_{\rm pow} - \left(\frac{\alpha_s}{\pi}\right) 0.161$	$-0.712\vert_{\rm pow} + \left(\frac{\alpha_s}{\pi}\right) 0.0365$
$\xi_{\rm NP}^{\langle T, T\rangle}$	$-77.960\vert_{\rm LO} + 9.734\vert_{\rm pow} + \left(\frac{\alpha_s}{\pi}\right) 15.260$	$0.023\vert_{\rm LO} - 1.120\vert_{\rm pow} + \left(\frac{\alpha_s}{\pi}\right) 6.887$	$71.831\vert_{\rm LO} - 7.041\vert_{\rm pow} - \left(\frac{\alpha_s}{\pi}\right) 49.633$
$\xi_{\rm NP}^{\langle V_L, V_R\rangle}$	$0.364\vert_{\rm LO} - 0.660\vert_{\rm pow} + \left(\frac{\alpha_s}{\pi}\right) 2.864$	$-0.278\vert_{\rm LO} - 0.119\vert_{\rm pow} - \left(\frac{\alpha_s}{\pi}\right) 0.462$	$-0.572\vert_{\rm LO} - 0.266\vert_{\rm pow} - \left(\frac{\alpha_s}{\pi}\right) 0.672$
$\xi_{\rm NP}^{\langle S_L, S_R\rangle}$	$0.182\vert_{\rm LO} + 1.503\vert_{\rm pow} + \left(\frac{\alpha_s}{\pi}\right) 0.553$	$-0.139\vert_{\rm LO} + 0.234\vert_{\rm pow} - \left(\frac{\alpha_s}{\pi}\right) 0.657$	$-0.286\vert_{\rm LO} - 1.208\vert_{\rm pow} + \left(\frac{\alpha_s}{\pi}\right) 0.315$
$\xi_{\rm NP}^{\langle S_L, T\rangle}$	$9.745\vert_{\rm LO} + 0.575\vert_{\rm pow} + \left(\frac{\alpha_s}{\pi}\right) 9.652$	$-0.0029\vert_{\rm LO} + 0.739\vert_{\rm pow} - \left(\frac{\alpha_s}{\pi}\right) 0.279$	$-8.978\vert_{\rm LO} + 1.011\vert_{\rm pow} - \left(\frac{\alpha_s}{\pi}\right) 5.528$
$\xi_{\rm NP}^{\langle S_R, T\rangle}$	$0.624\vert_{\rm pow}$	$0.348\vert_{\rm pow}$	$0.780\vert_{\rm pow}$

Table 5: Numerical values of the coefficients ξ in Eq. 26 for the lepton energy moments. We consider $E_\ell^{\rm cut} = 1$ GeV.

	$\langle M_X \rangle \cdot 10^{-1}$	$\langle (M_X - \langle M_X \rangle)^2 \rangle \cdot 10^{-1}$	$\langle (M_X - \langle M_X \rangle)^3 \rangle \cdot 10^{-1}$
$\xi_{\rm SM}$	$43.016\vert_{\rm LO} + 0.0648\vert_{\rm pow} + (\frac{\alpha_s}{\pi}) 7.219$	$2.232\vert_{\rm LO} + 7.417\vert_{\rm pow} + (\frac{\alpha_s}{\pi}) 29.666$	$-0.211\vert_{\rm LO} + 49.523\vert_{\rm pow} - (\frac{\alpha_s}{\pi}) 53.141$
$\xi_{\rm NP}^{\langle V_R, V_R\rangle}$	$1.221\vert_{\rm LO} - 1.680\vert_{\rm pow} - (\frac{\alpha_s}{\pi}) 0.925$	$-0.554\vert_{\rm LO} + 3.466\vert_{\rm pow} - (\frac{\alpha_s}{\pi}) 0.747$	$0.019\vert_{\rm LO} + 1.586\vert_{\rm pow} - (\frac{\alpha_s}{\pi}) 11.023$
$\xi_{\rm NP}^{\langle S_L, S_L\rangle}$	$-0.600\vert_{\rm LO} - 0.7916\vert_{\rm pow} - (\frac{\alpha_s}{\pi}) 2.041$	$0.0421\vert_{\rm LO} - 0.853\vert_{\rm pow} - (\frac{\alpha_s}{\pi}) 0.947$	$0.130\vert_{\rm LO} - 2.751\vert_{\rm pow} - (\frac{\alpha_s}{\pi}) 5.180$
$\xi_{\rm NP}^{\langle S_R, S_R\rangle}$	$-0.600\vert_{\rm LO} - 0.7916\vert_{\rm pow} - (\frac{\alpha_s}{\pi}) 2.041$	$0.042\vert_{\rm LO} - 0.853\vert_{\rm pow} - (\frac{\alpha_s}{\pi}) 0.947$	$0.130\vert_{\rm LO} - 2.751\vert_{\rm pow} - (\frac{\alpha_s}{\pi}) 5.180$
$\xi_{\rm NP}^{\langle T, T\rangle}$	$7.911\vert_{\rm LO} + 7.594\vert_{\rm pow} + (\frac{\alpha_s}{\pi}) 1.926$	$0.492\vert_{\rm LO} + 12.059\vert_{\rm pow} + (\frac{\alpha_s}{\pi}) 10.068$	$-1.620\vert_{\rm LO} + 39.365\vert_{\rm pow} + (\frac{\alpha_s}{\pi}) 20.575$
$\xi_{\rm NP}^{\langle V_L, V_R\rangle}$	$-2.134\vert_{\rm LO} + 2.182\vert_{\rm pow} - (\frac{\alpha_s}{\pi}) 0.274$	$0.364\vert_{\rm LO} - 5.449\vert_{\rm pow} - (\frac{\alpha_s}{\pi}) 0.137$	$0.404\vert_{\rm LO} - 8.685\vert_{\rm pow} + (\frac{\alpha_s}{\pi}) 5.821$
$\xi_{\rm NP}^{\langle S_L, S_R\rangle}$	$-1.067\vert_{\rm LO} - 1.616\vert_{\rm pow} - (\frac{\alpha_s}{\pi}) 3.189$	$0.182\vert_{\rm LO} - 0.811\vert_{\rm pow} - (\frac{\alpha_s}{\pi}) 1.786$	$0.202\vert_{\rm LO} - 4.346\vert_{\rm pow} - (\frac{\alpha_s}{\pi}) 9.340$
$\xi_{\rm NP}^{\langle S_L, T\rangle}$	$0.213\vert_{\rm LO} - 0.215\vert_{\rm pow} + (\frac{\alpha_s}{\pi}) 0.890$	$-0.145\vert_{\rm LO} + 1.040\vert_{\rm pow} + (\frac{\alpha_s}{\pi}) 0.018$	$-0.058\vert_{\rm LO} + 0.656\vert_{\rm pow} + (\frac{\alpha_s}{\pi}) 3.876$
$\xi_{\rm NP}^{\langle S_R, T\rangle}$	$-0.081\vert_{\rm pow}$	$0.327\vert_{\rm pow}$	$0.193\vert_{\rm pow}$

Table 6: Numerical values of the coefficients ξ in 26 for the hadronic invariant mass moments. We consider $E_\ell^{\rm cut} = 1$ GeV.

	$\langle q^2 \rangle$	$\langle (q^2 - \langle q^2 \rangle)^2 \rangle$	$\langle (q^2 - \langle q^2 \rangle)^3 \rangle$
$\xi_{\rm SM}$	$7.072\vert_{\rm LO} - 0.449\vert_{\rm pow} + (\frac{\alpha_s}{\pi})\, 0.168$	$4.278\vert_{\rm LO} - 1.727\vert_{\rm pow} + (\frac{\alpha_s}{\pi})\, 0.854$	$3.773\vert_{\rm LO} - 4.695\vert_{\rm pow} + (\frac{\alpha_s}{\pi})\, 6.879$
$\xi_{\rm NP}^{\langle V_R, V_R \rangle}$	$-0.681\vert_{\rm LO} + 0.138\vert_{\rm pow} + (\frac{\alpha_s}{\pi})\, 0.121$	$-1.231\vert_{\rm LO} + 0.429\vert_{\rm pow} + (\frac{\alpha_s}{\pi})\, 1.467$	$0.486\vert_{\rm LO} - 0.136\vert_{\rm pow} + (\frac{\alpha_s}{\pi})\, 5.182$
$\xi_{\rm NP}^{\langle S_L, S_L \rangle}$	$0.135\vert_{\rm LO} + 0.182\vert_{\rm pow} + (\frac{\alpha_s}{\pi})\, 0.373$	$0.099\vert_{\rm LO} + 0.592\vert_{\rm pow} + (\frac{\alpha_s}{\pi})\, 0.379$	$-0.512\vert_{\rm LO} + 1.236\vert_{\rm pow} - (\frac{\alpha_s}{\pi})\, 0.789$
$\xi_{\rm NP}^{\langle S_R, S_R \rangle}$	$0.135\vert_{\rm LO} + 0.182\vert_{\rm pow} + (\frac{\alpha_s}{\pi})\, 0.373$	$0.099\vert_{\rm LO} + 0.592\vert_{\rm pow} + (\frac{\alpha_s}{\pi})\, 0.379$	$-0.512\vert_{\rm LO} + 1.236\vert_{\rm pow} - (\frac{\alpha_s}{\pi})\, 0.789$
$\xi_{\rm NP}^{\langle T, T \rangle}$	$-2.174\vert_{\rm LO} + 0.510\vert_{\rm pow} + (\frac{\alpha_s}{\pi})\, 0.535$	$-1.591\vert_{\rm LO} + 1.290\vert_{\rm pow} - (\frac{\alpha_s}{\pi})\, 0.275$	$8.200\vert_{\rm LO} - 1.716\vert_{\rm pow} - (\frac{\alpha_s}{\pi})\, 10.168$
$\xi_{\rm NP}^{\langle V_L, V_R \rangle}$	$0.692\vert_{\rm LO} - 0.108\vert_{\rm pow} - (\frac{\alpha_s}{\pi})\, 0.090$	$0.765\vert_{\rm LO} - 0.248\vert_{\rm pow} - (\frac{\alpha_s}{\pi})\, 1.327$	$-2.109\vert_{\rm LO} + 0.814\vert_{\rm pow} - (\frac{\alpha_s}{\pi})\, 2.351$
$\xi_{\rm NP}^{\langle S_L, S_R \rangle}$	$0.346\vert_{\rm LO} + 0.359\vert_{\rm pow} + (\frac{\alpha_s}{\pi})\, 0.759$	$0.382\vert_{\rm LO} + 1.152\vert_{\rm pow} + (\frac{\alpha_s}{\pi})\, 0.557$	$-1.05\vert_{\rm LO} + 2.492\vert_{\rm pow} - (\frac{\alpha_s}{\pi})\, 2.439$
$\xi_{\rm NP}^{\langle S_L, T \rangle}$	0	0	0
$\xi_{\rm NP}^{\langle S_R, T \rangle}$	0	0	0

Table 7: Numerical values of the coefficients ξ in Eq. 26 for the q^2 moments. We consider $q^2_{\rm cut} = 4$ GeV^2.

References

[1] M. Bordone, B. Capdevila and P. Gambino, *Three loop calculations and inclusive Vcb*, *Phys. Lett. B* **822** (2021) 136679 [2107.00604].

[2] F. Bernlochner, M. Fael, K. Olschewsky, E. Persson, R. van Tonder, K. K. Vos et al., *First extraction of inclusive V_{cb} from q^2 moments*, 2205.10274.

[3] B. Grinstein and A. Kobach, *Model-Independent Extraction of $|V_{cb}|$ from $\bar{B} \to D^* \ell \overline{\nu}$*, *Phys. Lett. B* **771** (2017) 359 [1703.08170].

[4] F. U. Bernlochner, Z. Ligeti and D. J. Robinson, *N = 5, 6, 7, 8: Nested hypothesis tests and truncation dependence of $|V_{cb}|$*, *Phys. Rev. D* **100** (2019) 013005 [1902.09553].

[5] P. Gambino, M. Jung and S. Schacht, *The V_{cb} puzzle: An update*, *Phys. Lett. B* **795** (2019) 386 [1905.08209].

[6] P. Gambino et al., *Challenges in semileptonic B decays*, *Eur. Phys. J. C* **80** (2020) 966 [2006.07287].

[7] C. Bobeth, M. Bordone, N. Gubernari, M. Jung and D. van Dyk, *Lepton-flavour non-universality of $\bar{B} \to D^* \ell \bar{\nu}$ angular distributions in and beyond the Standard Model*, *Eur. Phys. J. C* **81** (2021) 984 [2104.02094].

[8] Fermilab Lattice, MILC collaboration, *Semileptonic form factors for $B \to D^* \ell \nu$ at nonzero recoil from 2 + 1-flavor lattice QCD*, 2105.14019.

[9] G. Martinelli, S. Simula and L. Vittorio, *Exclusive determinations of $|V_{cb}|$ and $R(D^*)$ through unitarity*, 2109.15248.

[10] P. Colangelo and F. De Fazio, *Tension in the inclusive versus exclusive determinations of $|V_{cb}|$: a possible role of new physics*, *Phys. Rev. D* **95** (2017) 011701 [1611.07387].

[11] M. Jung and D. M. Straub, *Constraining new physics in $b \to c \ell \nu$ transitions*, *JHEP* **01** (2019) 009 [1801.01112].

[12] A. Crivellin and S. Pokorski, *Can the differences in the determinations of V_{ub} and V_{cb} be explained by New Physics?*, *Phys. Rev. Lett.* **114** (2015) 011802 [1407.1320].

[13] T. Mannel, A. V. Rusov and F. Shahriaran, *Inclusive semitauonic B decays to order $\mathcal{O}(\Lambda_{QCD}^3/m_b^3)$*, *Nucl. Phys. B* **921** (2017) 211 [1702.01089].

[14] B. Dassinger, R. Feger and T. Mannel, *Complete Michel Parameter Analysis of inclusive semileptonic $b \to c$ transition*, *Phys. Rev. D* **79** (2009) 075015 [0803.3561].

[15] S. Turczyk, *Additional Information on Heavy Quark Parameters from Charged Lepton Forward-Backward Asymmetry*, *JHEP* **04** (2016) 131 [1602.02678].

[16] F. Herren, *The forward-backward asymmetry and differences of partial moments in inclusive semileptonic B decays*, 2205.03427.

[17] EOS Authors collaboration, *EOS: a software for flavor physics phenomenology*, *Eur. Phys. J. C* **82** (2022) 569 [2111.15428].

[18] R. Mandal, C. Murgui, A. Peñuelas and A. Pich, *The role of right-handed neutrinos in $b \to c\tau\bar{\nu}$ anomalies*, *JHEP* **08** (2020) 022 [2004.06726].

[19] B. Grzadkowski, M. Iskrzynski, M. Misiak and J. Rosiek, *Dimension-Six Terms in the Standard Model Lagrangian*, *JHEP* **10** (2010) 085 [1008.4884].

[20] J. Aebischer, A. Crivellin, M. Fael and C. Greub, *Matching of gauge invariant dimension-six operators for $b \to s$ and $b \to c$ transitions*, *JHEP* **05** (2016) 037 [1512.02830].

[21] A. V. Manohar and M. B. Wise, *Heavy quark physics*, vol. 10. 2000.

[22] B. M. Dassinger, T. Mannel and S. Turczyk, *Inclusive semi-leptonic B decays to order $1/m_b^4$*, *JHEP* **03** (2007) 087 [hep-ph/0611168].

[23] T. Mannel and K. K. Vos, *Reparametrization Invariance and Partial Re-Summations of the Heavy Quark Expansion*, *JHEP* **06** (2018) 115 [1802.09409].

[24] M. Fael, T. Mannel and K. Keri Vos, *V_{cb} determination from inclusive $b \to c$ decays: an alternative method*, *JHEP* **02** (2019) 177 [1812.07472].

[25] T. Mannel, S. Turczyk and N. Uraltsev, *Higher Order Power Corrections in Inclusive B Decays*, *JHEP* **11** (2010) 109 [1009.4622].

[26] P. Gambino, K. J. Healey and S. Turczyk, *Taming the higher power corrections in semileptonic B decays*, *Phys. Lett. B* **763** (2016) 60 [1606.06174].

[27] A. Celis, M. Jung, X.-Q. Li and A. Pich, *Scalar contributions to $b \to c(u)\tau\nu$ transitions*, *Phys. Lett. B* **771** (2017) 168 [1612.07757].

[28] A. Czarnecki, K. Melnikov and N. Uraltsev, *NonAbelian dipole radiation and the heavy quark expansion*, *Phys. Rev. Lett.* **80** (1998) 3189 [hep-ph/9708372].

[29] M. Jezabek and J. H. Kuhn, *QCD Corrections to Semileptonic Decays of Heavy Quarks*, *Nucl. Phys. B* **314** (1989) 1.

[30] M. Jezabek and L. Motyka, *Tau lepton distributions in semileptonic B decays*, *Nucl. Phys. B* **501** (1997) 207 [hep-ph/9701358].

[31] F. De Fazio and M. Neubert, *$B \to X_u l \bar{\nu}_l$ decay distributions to order α_s*, *JHEP* **06** (1999) 017 [hep-ph/9905351].

[32] M. Trott, *Improving extractions of $|V_{cb}|$ and m_b from the hadronic invariant mass moments of semileptonic inclusive B decay*, *Phys. Rev. D* **70** (2004) 073003 [hep-ph/0402120].

[33] V. Aquila, P. Gambino, G. Ridolfi and N. Uraltsev, *Perturbative corrections to semileptonic b decay distributions*, *Nucl. Phys. B* **719** (2005) 77 [hep-ph/0503083].

[34] P. Gambino, G. Ossola and N. Uraltsev, *Hadronic mass and q^2 moments of charmless semileptonic B decay distributions*, *JHEP* **09** (2005) 010 [hep-ph/0505091].

[35] A. Alberti, P. Gambino, K. J. Healey and S. Nandi, *The Inclusive Determination of $|V_{cb}|$*, *Nucl. Part. Phys. Proc.* **273-275** (2016) 1325.

[36] V. Shtabovenko, R. Mertig and F. Orellana, *FeynCalc 9.3: New features and improvements*, *Comput. Phys. Commun.* **256** (2020) 107478 [2001.04407].

[37] J. Aebischer, M. Fael, C. Greub and J. Virto, *B physics Beyond the Standard Model at One Loop: Complete Renormalization Group Evolution below the Electroweak Scale*, *JHEP* **09** (2017) 158 [1704.06639].

[38] C. Anastasiou and K. Melnikov, *Higgs boson production at hadron colliders in NNLO QCD*, *Nucl. Phys. B* **646** (2002) 220 [hep-ph/0207004].

[39] S. A. Larin, *The Renormalization of the axial anomaly in dimensional regularization*, *Phys. Lett. B* **303** (1993) 113 [hep-ph/9302240].

[40] P. Gambino, *B semileptonic moments at NNLO*, *JHEP* **09** (2011) 055 [1107.3100].

[41] I. I. Y. Bigi, M. A. Shifman, N. Uraltsev and A. I. Vainshtein, *High power n of m_b in beauty widths and $n = 5 \to \infty$ limit*, *Phys. Rev. D* **56** (1997) 4017 [hep-ph/9704245].

[42] M. Fael, K. Schönwald and M. Steinhauser, *Kinetic Heavy Quark Mass to Three Loops*, *Phys. Rev. Lett.* **125** (2020) 052003 [2005.06487].

[43] M. Fael, K. Schönwald and M. Steinhauser, *Relation between the $\overline{\text{MS}}$ and the kinetic mass of heavy quarks*, *Phys. Rev. D* **103** (2021) 014005 [2011.11655].

[44] F. Herren and M. Steinhauser, *Version 3 of RunDec and CRunDec*, *Comput. Phys. Commun.* **224** (2018) 333 [1703.03751].

[45] M. González-Alonso, J. Martin Camalich and K. Mimouni, *Renormalization-group evolution of new physics contributions to (semi)leptonic meson decays*, *Phys. Lett. B* **772** (2017) 777 [1706.00410].

[46] Q.-Y. Hu, X.-Q. Li and Y.-D. Yang, *$b \to c\tau\nu$ transitions in the standard model effective field theory*, *Eur. Phys. J. C* **79** (2019) 264 [1810.04939].

[47] Belle collaboration, *Moments of the electron energy spectrum and partial branching fraction of B —> X(c) e nu decays at Belle*, *Phys. Rev. D* **75** (2007) 032001 [hep-ex/0610012].

[48] BaBar collaboration, *Measurement of the electron energy spectrum and its moments in inclusive $B \to Xe\nu$ decays*, *Phys. Rev. D* **69** (2004) 111104 [hep-ex/0403030].

[49] CLEO collaboration, *Moments of the B meson inclusive semileptonic decay rate using neutrino reconstruction*, *Phys. Rev. D* **70** (2004) 032002 [hep-ex/0403052].

[50] Belle collaboration, *Moments of the Hadronic Invariant Mass Spectrum in $B \to X_c\ell\nu$ Decays at BELLE*, *Phys. Rev. D* **75** (2007) 032005 [hep-ex/0611044].

[51] BaBar collaboration, *Measurement and interpretation of moments in inclusive semileptonic decays $\overline{B} \to X_c l\bar{\nu}u$*, *Phys. Rev. D* **81** (2010) 032003 [0908.0415].

[52] Belle-II collaboration, *Measurement of Hadronic Mass Moments $\langle M_X^n \rangle$ in $B \to X_c\ell\nu$ Decays at Belle II*, 2009.04493.

[53] Belle collaboration, *Measurements of q^2 Moments of Inclusive $B \to X_c\ell^+\nu_\ell$ Decays with Hadronic Tagging*, *Phys. Rev. D* **104** (2021) 112011 [2109.01685].

[54] Belle-II collaboration, *Measurement of Lepton Mass Squared Moments in $B \to X_c\ell\bar{\nu}_\ell$ Decays with the Belle II Experiment*, 2205.06372.

[55] M. Fael, K. Schönwald and M. Steinhauser, *A first glance to the kinematic moments of $B \to X_c\ell\nu$ at third order*, 2205.03410.

[56] P. D. Group, P. A. Zyla, R. M. Barnett, J. Beringer, O. Dahl, D. A. Dwyer et al., *Review of Particle Physics*, *Progress of Theoretical and Experimental Physics* **2020** (2020) .

[57] M. Rahimi and K. K. Vos, *Standard Model predictions for Lepton Flavour Universality ratios of inclusive semileptonic B decays*, 2207.03432.

[58] P. Gambino, A. Melis and S. Simula, *Extraction of heavy-quark-expansion parameters from unquenched lattice data on pseudoscalar and vector heavy-light meson masses*, *Phys. Rev. D* **96** (2017) 014511 [1704.06105].

[59] P. Gambino and S. Hashimoto, *Inclusive Semileptonic Decays from Lattice QCD*, *Phys. Rev. Lett.* **125** (2020) 032001 [2005.13730].

[60] P. Gambino, S. Hashimoto, S. Mächler, M. Panero, F. Sanfilippo, S. Simula et al., *Lattice QCD study of inclusive semileptonic decays of heavy mesons*, *JHEP* **07** (2022) 083 [2203.11762].

[61] A. Sirlin, *Radiative corrections to g(v)/g(mu) in simple extensions of the su(2) x u(1) gauge model*, *Nucl. Phys. B* **71** (1974) 29.